ADVANCED FUNCTIONAL MATERIALS
www.afm-journal.de

A Series of Hybrid Multifunctional Interfaces as Artificial SEI Layer for Realizing Dendrite Free, and Long-Life Sodium Metal Anodes

Megala Moorthy, Brindha Moorthy, Bala Krishnan Ganesan, Aditi Saha, Seungju Yu, Do-Hoon Kim, Seungbum Hong, Sangho Park, Kisuk Kang, Ranjith Thangavel, and Yun-Sung Lee**

Sodium metal (Na) anodes are considered the most promising anode for high-energy-density sodium batteries because of their high capacity and low electrochemical potential. However, Na metal anode undergoes uncontrolled Na dendrite growth, and unstable solid electrolyte interphase layer (SEI) formation during cycling, leading to poor coulombic efficiency, and shorter lifespan. Herein, a series of Na-ion conductive alloy-type protective interface (Na-In, Na-Bi, Na-Zn, Na-Sn) is studied as an artificial SEI layer to address the issues. The hybrid Na-ion conducting SEI components over the Na-alloy can facilitate uniform Na deposition by regulating Na-ion flux with low overpotential. Furthermore, density functional study reveals that the lower surface energy of protective alloys relative to bare Na is the key factor for facilitating facile ion diffusion across the interface. Na metal with interface layer facilitates a highly reversible Na plating/stripping for ≈790 h, higher than pristine Na metal (100 h). The hybrid self-regulating protective layers exhibit a high mechanical flexibility to promote dendrite free Na plating even at high current density (5 mA cm^{-2}), high capacity (10 mAh cm^{-2}), and good performance with $Na_3V_2(PO_4)_3$ cathode. The current study opens a new insight for designing dendrite Na metal anode for next generation energy storage devices.

1. Introduction

Recently, the worldwide demand for high energy density storage devices has increased massively owing to the development of automated systems in electrical and electronic fields such as microelectronics, electric vehicles (EVs), artificial intelligence, and grid storage energy storage systems (ESS).[1,2,3] Among the commercially available energy storage devices, batteries are considered the major storage medium for all portable devices, such as electric vehicles, mobile phones, laptops and medical electronic devices, which are ubiquitous in the modern digital era. Thus far, the lithium-ion battery (LIB) has been the primary energy-storage medium in such devices because of its superior performance compared to other types of batteries.[4,5] Most importantly, LIBs offers high energy, no memory effect, and have extremely low discharge rates, making them the optimum choice for large scale energy storage

M. Moorthy, B. K. Ganesan, Y.-S. Lee
School of Chemical Engineering
Chonnam National University
Gwangju 61186, Republic of Korea
E-mail: leeys@chonnam.ac.kr

B. Moorthy
Department of Chemical Engineering
Indian Institute of Technology Tirupati
Tirupati 517619, India

A. Saha, S. Hong
Department of Materials Science and Engineering
Korea Advanced Institute of Science and Technology (KAIST)
Daejeon 34141, Republic of Korea

S. Yu, D.-H. Kim, K. Kang
Department of Materials Science and Engineering
Seoul National University
Seoul 08826, Republic of Korea

S. Park
Department of Battery Engineering
Dongshin University
Dongshindae-gil 34-22, Jeollanam-do, Naju-si 58245, Republic of Korea

R. Thangavel
School of Energy Science and Engineering
Indian Institute of Technology Guwahati
Guwahati 781039, India
E-mail: ranjith.t@iitg.ac.in

The ORCID identification number(s) for the author(s) of this article can be found under https://doi.org/10.1002/adfm.202300135

DOI: 10.1002/adfm.202300135

applications such as EVs and ESS.[6]However, the extensive market demand of LIBs has increased the concerns due to global lithium resources shortage, leading to the high cost of Li resources, affecting the energy cost (USD/kWh) of LIBs. In this regard, extensive research is on progress to replace the LIBs with cheaper alternate with performance metrics equivalent to LIBs. Owing to the abundance (1200 times higher than Li resources), and similar working chemistry, sodium-ion batteries (SIBs) are the most appealing candidate for next generation applications.[7,8]As a result of intense research on SIBs, a variety of high voltage, and high capacity cathode materials based on layered oxides, and phosphates have been identified.[9] However, a developing an anode material with high capacity remains challenging because of graphite, the most successful anode in LIBs, do not support intercalation with Na^+ ions. Although, several high capacity metals, metal oxides, and metal sulfides were studied as the anode for SIBs, the working potential of the anode materials are not sufficient to a high energy density SIBs equivalent to LIBs.[10]

Na metal is regarded as the promising anode for high energy density sodium battery owing to its high theoretical capacity (1166 mAh g^{-1}) and extremely low electrochemical potential (−2.714 versus SHE). Therefore, SIBs employing Na metal anode can achieve high energy density equivalent to the commercial LIBs, and low energy cost.[11] Nonetheless, prior to the use of sodium batteries in practical applications, several limitations of sodium metal anodes such as stability, reversibility, and safety must be addressed. The Na metal is highly reactive with atmosphere, and it can react parasitically with organic electrolytes to naturally create a thick solid electrolyte interphase (SEI) layer over the surface of Na metal.[12]The naturally formed SEI layer is highly loose, unstable and does not remain homogenous during cycling, inducing uneven Na-ion diffusion and poor columbic efficiency. The natural SEI is highly uneven and fragile, resulting in uneven Na dendrite deposition, causing the natural SEI to crack and grow dendrites. In addition, Na deposition at high capacity and high current in 2D host-less Na anode can induce huge volume expansion, provoking internal stress over the SEI layer, leading to breaking/cracking of the SEI during the cycling process. The continuous depletion of SEI layer and formation of new SEI layer can consume a large amount of electrolyte, leading to electrolyte depletion and increase in internal cell resistance.[13,14] Moreover, the chain of unwanted reactions can lead to the severe dendrites formation, and dead Na formations which can reach the cathode through separator and cause short-circuit issues in the battery.[15]Therefore, formation of stable SEI over Na metal is crucial to extend the cycle life, and safety of metal anode. An ideal SEI over Na surface should have chemical and electrochemical stability along with high Na- ion conductivity. The components of the SEI layer should renders a constant Na-ion flux and even electric field distribution, and it holds the high flexibility, and robustness to direct smooth Na deposition/stripping.[16]

Several strategies have been adapted over Na metal anode to achieve a smooth and dendrite free Na deposition/stripping : i) Engineering the electrolytes with new formulations and addition of additives to reduces the reactivity of Na metal with electrolyte, and to improve the SEI layer stability ii) nanostructured current collectors and 3D host materials to minimize the local current density, and homogenize the Na-ion flux to achieve reduced volume expansion and dendrite free deposition during cycling; iii) constructing a interface layer or a Na-ion conductive "artificial" SEI layer with good mechanical strength to regulate the facile Na-ion transport to promote the uniform Na deposition.[17,18] In general, constructing a interface layer over Na metal surface is an efficient strategy to overcome the issues in Na metal anode as the interface layer could act as artificial barriers to lower electrochemical reactivity of Na metal, thus effectively suppressing the occurrence of side reactions. The SEI layer is still formed over the artificial SEI layer during initial cycling, but the SEI formation is much less reactive due to the presence of artificial layer over the metal anodes. The Na anodes with favorable interface layers show better tolerate against the volume changes during Na plating and stripping process.[19,20]

Several strategies such as depositing metal oxides (Al_2O_3, ZnO, Mxenes, etc.,), carbon skeletons (graphene, carbon fibers, doped carbon), alloy type interfaces (NaBr, $Na_{15}Sn$, $Sn_{0.9}Hg_{0.1}$), organic polymers (PVDF, PMMA, etc.,) have been utilized as interface/artificial SEI layer.[21] Unlike natural SEI layer, artificial SEI layer will be highly smooth and mechanically strong, resulting in smooth Na deposition without the crack and dendrites. Artificial SEI layers can allow facile Na-ion diffusion through SEI layer and enable Na metal deposit uniformly without dendrite formation. The naturally formed SEI layer over Na metal is highly heterogeneous due to contains a mixture of insoluble organic/inorganic products and possesses highly mosaic structure on the surface. The uneven thickness of the natural SEI layer and heterogeneous nature of naturally formed SEI will induce uneven Na-ion diffusion, poor columbic efficiency, dendrite formation, and SEI layer breakage. Moreover, the complex mosaic and heterogeneous nature of naturally formed SEI layer has poor ionic conductivity due to presence of composite phases and several interfacial defects. The inhomogeneity in natural SEI layer will accelerate the strong electric field across the Na anode with dendrite formation, reducing the ionic conductivity of SEI layer.[1] In contrast, artificial SEI layers are highly homogenous with high mechanical strength, good flexibility, and high Na- ion conductivity that can efficiently suppress the Na dendrite growth. However, by engineering the artificial SEI layer with favorable SEI components can promote homogenous Na ion flux, and improved Na-ion conductivity along with reduced nucleation over potential.[22] The formation of interface is very crucial as the thinner interface could catalyze unstable SEI growth while thicker interface provokes unacceptable Na-ion diffusion resistance. The interface layer should maintain mechanical integrity and should have flexibility to achieve a high capacity and high-rate sodium deposition. Moreover, the components of the SEI layer are very crucial to achieve a long-life Na anode with high capacity, high rate, and safety. The inorganic components of the artificial SEI layer could rupture during a huge volume change of Na metal under high current density, while the organic components of artificial SEI layer will impede the high-capacity storage of Na metal due to poor Na-ion diffusion pathways.[22] A Hybrid multifunctional artificial SEI layer is very crucial to realize dendrite free Na metal anodes at high current and high-capacity condition.[23]

Herein, we address the issues in Na metal anodes by developing a series of Na-ion conductive alloy-type (Na-In, Na-Bi, Na-Zn, Na-Sn) hybrid artificial SEI layer through a facile in situ solvent-based strategy. The controlled self-alloying reaction between the

Na-metal and alloy components, a sodium metal alloy interphase (Na-M) is generated close to the sodium metal anode, which can reduce the resistance between Na metal and the electrolyte. The Na metal anode with alloy layer and hybrid Na-ion conducting organic-inorganic SEI components can facilitate uniform Na deposition in metal anodes by regulating the Na-ion flux with a low overpotential. It also revealed that the lower surface energy of the Na-alloys relative to pristine Na metal was the key factor for facilitating facile Na-ion diffusion across the interface. Moreover, the sodium deposition in alloy layers with hybrid SEI components is inclined toward the particular planes of alloy surface. Na metal anodes with protective interface can be cycled over 790 h in a symmetrical cell with low overpotential (11 mV), higher than pristine Na metal (73 mV after 100 h). Furthermore, the mechanical strength of the alloy interface also influences the cycle life of the Na metal anode and the stability of the Na metal increases in the following order (Na<NaBi<NaZn<NaSn<NaIn).The high mechanical flexibility from hybrid self-regulating alloy – inorganic NaCl SEI–organic SEI protective layers promoted dendrite free behavior, even at high current density (5 mA cm^{-2}), and high capacity (5 mAh cm^{-2}). The feasibility of the protected metal anode was tested in full-cell conditions by coupling with $Na_3V_2(PO_4)_3$ cathode, and the protected anode performs remarkably well with low polarization, high coulombic efficiency, and long cycle life than pristine Na anode, indicating the potential of commercial feasibility. These findings are expected to advance the development of dendrite free Na metal anode by highlighting that a multifunctional approach to designing the hybrid artificial SEI components of the Na anode plays a key role in achieving the long life and safer of sodium metal batteries.

2. Experimental Section

2.1. Chemicals and Materials

Following materials were used in the experimental process: Sodium metal cubes (99.9%, Sigma Aldrich), Indium chloride ($InCl_3$, Sigma Aldrich, 98%), Bismuth chloride ($BiCl_3$, Alfa Aesar, 99.9%),Tin chloride ($SnCl_2$, Alfa Aesar, 99%), Zinc chloride ($ZnCl_2$, Duksan, 98.9%), Tetrahydrofuran solvent (THF Junsei Chemical).

2.2. Fabrication of Protective Coating Alloy Layer

The solution for forming the alloy layer over Na anode was prepared by dissolving 0.15 M anhydrous metal chloride ($InCl_3$ or other required metal chloride) salt in tetrahydrofuran solvent. THF was the most widely used universal organic solvent for fabricating protective coating alloy layers on sodium metal surfaces, because it has a low boiling point of 66 °C.[24] The dried sodium metal cubes were cut into the circular disk of 12 mm diameter, polished well, and the metal chloride solution was drop casted on the surface of the sodium metal. The metal chloride solution reacts with sodium metal to form the corresponding Na–metal alloy layer. The protective alloy layer over Na metal was formed through the self-alloying reaction between sodium metal and metal chloride solution. Then, the Na metal was dried inside the glovebox to evaporate any residual solvent and the alloy coated Na metal anode was directly used for physical and electrochemical characterization. The abovementioned process was executed in a glove box filled with Ar gas.

2.3. Material Characterization

Physical characterization, chemical characterization, and morphological studies of all Na metal and Na anodes with protective layers were studied with extreme precautions to avoid exposure of sodium metal to air and moisture. A high-resolution X-ray diffractometer (Pan Analytical) equipped with a Cu-Kα radiation source was used to analyze the crystal phase. A Kapton Tape was used to cover the Na-M alloy to avoid exposure of sodium metal to air and moisture. The morphologies of the alloy layer and sodium dendrites on the surface were analyzed using a FE-SEM (S4700, Hitachi, Japan) equipped with an energy-dispersive spectrometer (EDX). The samples processed and stored in a closed container inside glovebox and immediately transferred to SEM chamber during analysis. The chemical composition and oxidation states of various metals in this study, Thermo VG Scientific X-ray photoelectron spectroscopy (XPS) was used. Nanoindentation studies were carried out using a commercial atomic force microscope (MFP-3D Origin AFM with Standard holder and an electrical closed cell, Oxford Instruments Asylum Research Inc., USA) in Argon gas (99.999%) environment. A nonconductive type of diamond-coated tip (DT-NCHR, resonance frequency 400 kHz by Nanoworld) with a high spring constant (80 N m^{-1}) was used for the topography imaging as well as nanoindentation measurements. With a loading force of 3 μN, over 10 μm by 10 μm surface area, the average Young's modulus of the electrode samples was calculated based on the Hertzian model of nanoindentation.

2.4. Electrochemical Characterization

The pristine Na metal anode (12 mm diameter) and alloy coated Na metal anode (12 mm diameter) after fabrication process, it was directly tested in a symmetric cell configuration using a CR2032 coin-cell. The coin-cells were assembled inside a glove box with sodium hexafluorophosphate ($NaPF_6$) in DIGLYME as electrolyte and Polypropylene (Celgard) membrane was used as the separator. The symmetrical cell performance was investigated in a galvanostatic mode at various current densities, and various discharge capacity using a WBS3000 Wonatech battery cycler. A full cell was constructed using pristine Na anode or Na metal anode with alloy interface and $Na_3V_2(PO_4)_3$ cathode. The full-cell was assembled in a CR2032 coin-cell with 1 M $NaPF_6$ in DIGLYME as the electrolyte, and polypropylene separator. The mass loading of $Na_3V_2(PO_4)_3$ cathode was ≈10 mg cm^{-2}. The galvanostatic performance of the cell was analyzed using a WBS3000 Wonatech battery cycler in the voltage range of 1–3.8 V.

2.5. DFT Calculation

All the first-principles calculations were performed based on the density functional theory (DFT), and they were implemented

using the Vienna ab initio Simulation Package (VASP).[25] The projector-augmented wave (PAW) pseudopotentials were used.[26] An energy cutoff of 500 eV and 2 × 2 × 1 k-point grid was used for all the calculations based on the Monkhorst–Pack scheme .[27]The surfaces were created with at least six layers of metal alloy, along with a vacuum layer of 12 Å. A residual force of 0.02 eV $Å^{-1}$ was used as the criterion for structural relaxation. To evaluate the activation barrier of Na-ion diffusion, the climbing image nudged elastic band (CI-NEB) method was applied to five images along the diffusion pathway.[28]

3. Results and discussion

The alloy type protective interface layer was constructed on a Na metal surface by a facile self-alloying reaction between Na metal and metal chloride solution. The alloy interface layers are thin and chemically bond to the Na metal surface during the in situ chemical reduction of metal chlorides by Na metal.[25] The formation of the alloy type protective layer over Na metal surface proceeds through the following reactions to form a thermodynamically favorable phase: i) $xNa + MCl_x \rightarrow M + xNaCl$ (M = In, Bi, Sn, Zn), ii) $yNa + zM \rightarrow Na_y M_z$. The reaction continues until a single-phase alloy layer is formed over the Na metal anode. The reaction of alloy layer formation is fast, and the surface color of Na metal turns to black color, as depicted in the photographic images (Figure S1a–e, Supporting Information) immediately on drop casting of the solution. The high-resolution XRD in (**Figure 1**a), indicates the formation of the following Na-metal alloy phases over the Na metal surface: Na_1In_1, Na_1Bi_1, Na_1Zn_{13}, and Na_1Sn_2 when treated with the corresponding metal chloride solution. The sharp peaks indicate the crystalline nature of the alloy layer over Na metal, and no other impurity phases are noted.[23]The chemical composition of the freshly prepared Na metal anode with the protective alloy layer was analyzed using XPS. The Na anode with Na_1In_1 protective alloy exhibits characteristic In 3d spectrum which can be deconvoluted into two peaks at 446.27 eV (In $3d_{5/2}$) and 453.36 eV (In $3d_{3/2}$) (Figure 1b). Some components of metal (In^0) and metal oxides (In_2O_3) were also observed and could be formed during the sample handling process.[29] Moreover, the presence of Na-rich SEI layer component (NaCl) over Na_1In_1 alloy is evidenced by signals from the Cl 2p characteristic spectrum (Figure 1c) and the two peaks at 198.2 eV and 200.3 eV in the Cl 2p spectrum were assigned to Cl $2p_{3/2}$ and Cl $2p_{1/2}$ respectively. SEM images of Na, Na_1In_1,

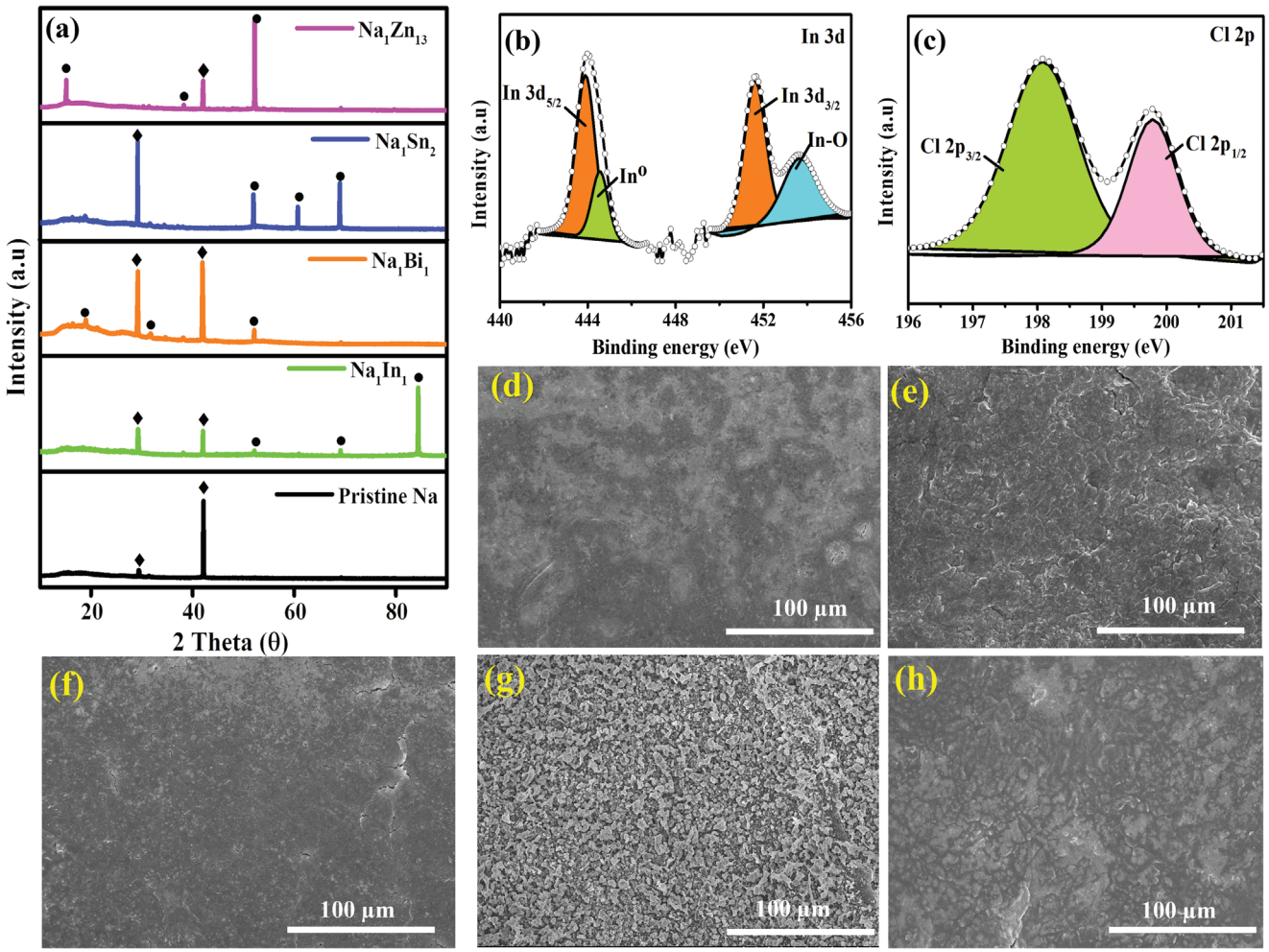

Figure 1. a) XRD diffraction patterns of sodium metal and alloy protected Na anodes, De-convoluted XPS spectrum from Na_1In_1 anode b) In 3d, and c) Cl 2p, Surface SEM images of d) Pristine Na, and Na protected with e) Na_1In_1, f) Na_1Bi_1 , g) Na_1Sn_2, and h) Na_1Zn_{13}

Na_1Bi_1, Na_1Zn_{13}, and Na_1Sn_2 alloy surface in (Figure 1d–h) show the formation of the new alloy layer over the Na metal after facile chemical solvent modification approach. The morphology of the alloy layer formed over the Na metal surface is different for each alloy. This is mainly attributed due to defects during room-temperature growth of the alloys during the chemical reduction of Na metal.[30] The cross section SEM images (Figure S2a,b, Supporting Information) of the Na_1In_1 alloy layer show the presence of the composite alloy layer of ≈10–13 µm thickness. The Energy dispersive spectroscopy (EDAX) mapping before cycling of the Na_1In_1 film shows a uniform distribution of In and Cl over the Na layer (Figure S2c–f, Supporting Information) and the Cl is attributed due to the formation of sodium rich NaCl phase over Na metal during the alloy formation.

3.1. Understanding the Na deposition in Na metal anode with Alloy Interface Layer

A constant amount of Na was galvanostatically deposited (2 mAh cm^{-2} at 2 mA cm^{-2}) onto the pristine Na anode and Na anode with alloy interface to probe the sodium deposition and dendrite formation process. The SEM images (Figure S3, Supporting Information) shows that Na plating is highly inhomogeneous with agglomerated and rough deposits over pristine Na metal. Such rough Na deposits over pristine Na metal is occurred due to inhomogeneous local current distribution that provoke non-uniform Na^+ ion flux.[31] The Na^+ ion seeding process in pristine Na metal has to overcome higher nucleation energy barrier, provoking the dendrite deposition in host-less Na metal. Such uneven Na deposition will induce severe side reactions between Na metal and the electrolyte, decreasing the coulombic efficiency of the cell.[32] However, the Na deposition over Na metal with Na_1In_1 alloy shows the uniform, and smoother deposition without formation of dendrites on the surface (**Figure 2**a). The smoother Na deposition without dendrites will reduce the unwanted electrolyte reaction with Na metal, leading to increased cycle life of the alloy protected metal anodes.[33]The cross-sectional SEM images of Na anode with Na_1In_1 layer indicates the Na deposition (bright layer) is beneath the Na_1In_1 alloy layer, and the thickness of the deposited Na metal is ≈10 µm (Figure 2b,c). The top Na_1In_1 alloy layer is generally comprised of several Na-rich organic and inorganic SEI components with higher electron densities than Na metal, the top dark layer in the cross-sectional SEM corresponds to the Na_1In_1 alloy layer, whereas the bottom bright layer represents the Na deposits. The Na deposition below the Na_1In_1 alloy layer is mainly attributed to difference in the sodio-philicity and insulative properties of the hybrid alloy layer, and the SEI components over the metal anode. The Na-M alloy phases are likely to be electronic conductors or semiconductors but the NaCl formed as byproduct over Na-M alloy phase is highly insulating, making the hybrid artificial SEI layer highly resistive.[3] Such highly resistance layer were previously studied in several protective layers and were even explored in some amorphous carbons and graphene based protective layers. The protective alloy layer possesses the lowest activation barrier and can facilitate a high potential gradient and rapid diffusion of sodium ions across the interphases. This unique feature of the hybrid SEI layer is sufficient enough to develop an electric field across the protective film, providing a driving force for Na-ion diffuse through the artificial SEI layer, and induces Na plating underneath the Na-M alloy interface layer.[34,35]

The Na anode with Na_1In_1 alloy layer maintained a smoother Na deposition without dendrites even at high Na deposition capacity (5 mAh cm^{-2}). SEM images in (Figure 2d–f) shows that the Na metal with Na_1In_1 alloy layer efficiently handled the Na deposition without any deleterious volume changes due to less reactivity of the Na_1In_1 layer with electrolyte due to their lower chemical potential.[36] The high mechanical strength of the alloy layer with hybrid SEI components can efficiently withstand volume expansion during high Na deposition process.[37]At higher Na deposition capacity (10 mAh cm^{-2}), a slight breakage of the Na_1In_1 protective alloy layer is noted and Na deposition takes over the alloy layer (Figure 2g–i). This is attributed to the inability of the thin alloy layer to infiltrate and holds more Na deposition at high capacity. However, no mossy and inhomogeneous dendrite deposits are noted over Na anode protected with Na_1In_1 alloy even under such high capacity deposition.[38] Even at high current density (5 mA cm^{-2}) Na anode protected with Na_1In_1 alloy showed smooth Na plating and stripping due reduction in effective current density, suppressing the dendritic growth (Figure 2j–l). In contrast, pristine Na metal showed significant damages, the size of the dendrites and surface roughness of deposited Na metal increased over pristine Na anode at high current and high capacity (Figure S3, Supporting Information). The dendrites grow vertically over pristine Na anode due to irregular amorphous grains that maximize the local current density. Such large Na dendrites formation over Na metal is highly dangerous, as it could puncture the separator, provoking the internal short circuit.[39,40] The SEM images (Figure S4, Supporting Information) of Na anode with other alloy layers (Na_1Bi_1, Na_1Zn_{13}, and Na_1Sn_2) showed a smoother Na deposition without dendrites at low deposition capacity and current density (2 mA cm^{-2}, 2 mAh cm^{-2}), which clearly explains that the combination of multi-interface layer benefits to the fast sodium diffusion and smoother deposition.

3.2. Electrochemical Study of Na Metal Anodes

To verify the effectiveness of the protective alloy layer on Na metal, the pristine Na metal, and alloy protective Na metal were cycled in the symmetrical cell configuration at an aerial capacity of 2 mAh cm^{-2} and a current density of 2 mA cm^{-2} (**Figure 3**a). The voltage profile of pristine Na anode shows high overpotential (63 mV) than Na anode with protective alloy, and the overpotential gradually increases upon cycling (74 mV after 120 h), followed by rigorous voltage fluctuations and the cell failure. The continuous increase in polarization of pristine Na anode with cycling is mainly attributed to unstable interface and parasitic reactions between Na metal and the electrolyte, leading to continuous breakage/formation of the SEI layer. The voltage fluctuations are associated with sudden cell failure, originating from Na dendrite penetration and short-circuiting.[11] In contrast, Na metal anode with alloy protective layer shows a very stable voltage profile without any fluctuations. Na anode with Na_1In_1 alloy layer showed the lowest overpotential of 11 mV and could cycle for more than 790 h without short-circuit. These electrochemical tests indicate that the protective alloy interface over Na anode increased the

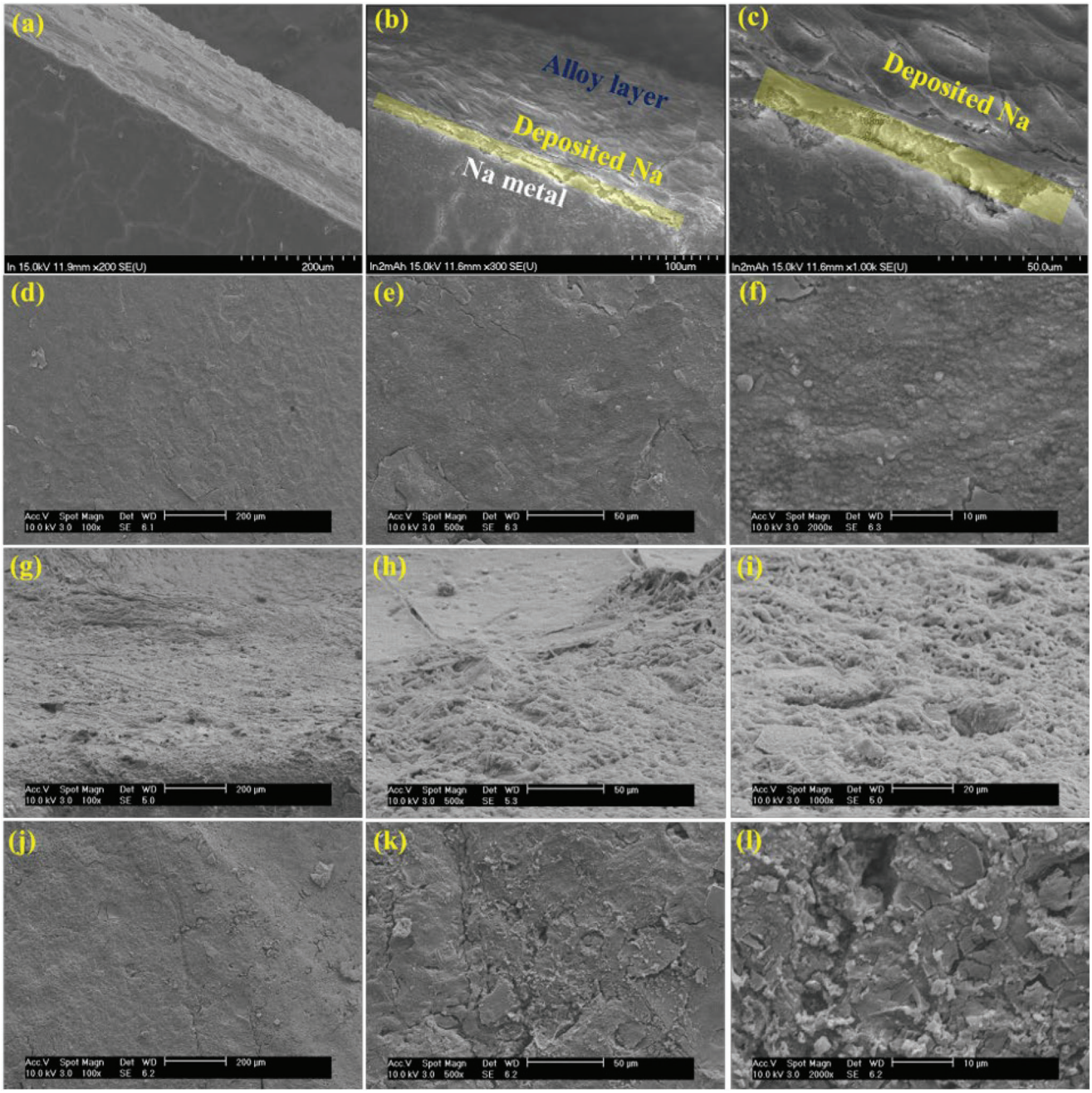

Figure 2. a–c) Cross-sectional SEM images of Na_1In_1 deposited with 2 mAh cm^{-2} at 2 mA cm^{-2} of Na, and SEM images of Na_1In_1 with different Na deposition conditions d–f): 5 mAh cm^{-2} at 2 mA cm^{-2}, g–i) 10 mAh cm^{-2} at 2 mA cm^{-2} and j–l) 2 mAh cm^{-2} at 5 mA cm^{-2}.

stability of the SEI layer during the repeated Na plating/stripping process.[24] Meanwhile, Na_1Sn_2, Na_1Zn_{13}, Na_1Bi_1 protected Na anode can also be cycled efficiently with low overpotential, and polarization. The surface energy and diffusion barrier required for the Na^+ ion to diffusion reduces greatly, after the introduction of alloy layer, increasing the efficiency of Na anode.[41]

However, the cycling efficiency and overpotential of the different alloys varies significantly after 300 h. The cycle life of alloy protected Na anode increases in the following order (Na-Bi< Na-Zn<Na-Sn<Na-In) and can be efficiently cycled over 365 h, 446 h, 618 h, and 790 h respectively. Moreover, voltage profiles are zoomed-in and presented in (Figure 3b–e), and it is clearly evident from the voltage profiles, no fluctuation in voltage was observed for alloy protected Na anode even after prolonged cycling. This is mainly attributed to differentness in mechanical properties Na^+ ion diffusion co-efficient exhibited by the alloy layer.[20] The hybrid multifunctional interfaces are mechanically strong, due to the contribution from organic/inorganic layers with high young's modulus, thereby reducing the dendrite formation.[42] The overpotential of Na anode with Na-In, Na-Sn, Na-Zn, and

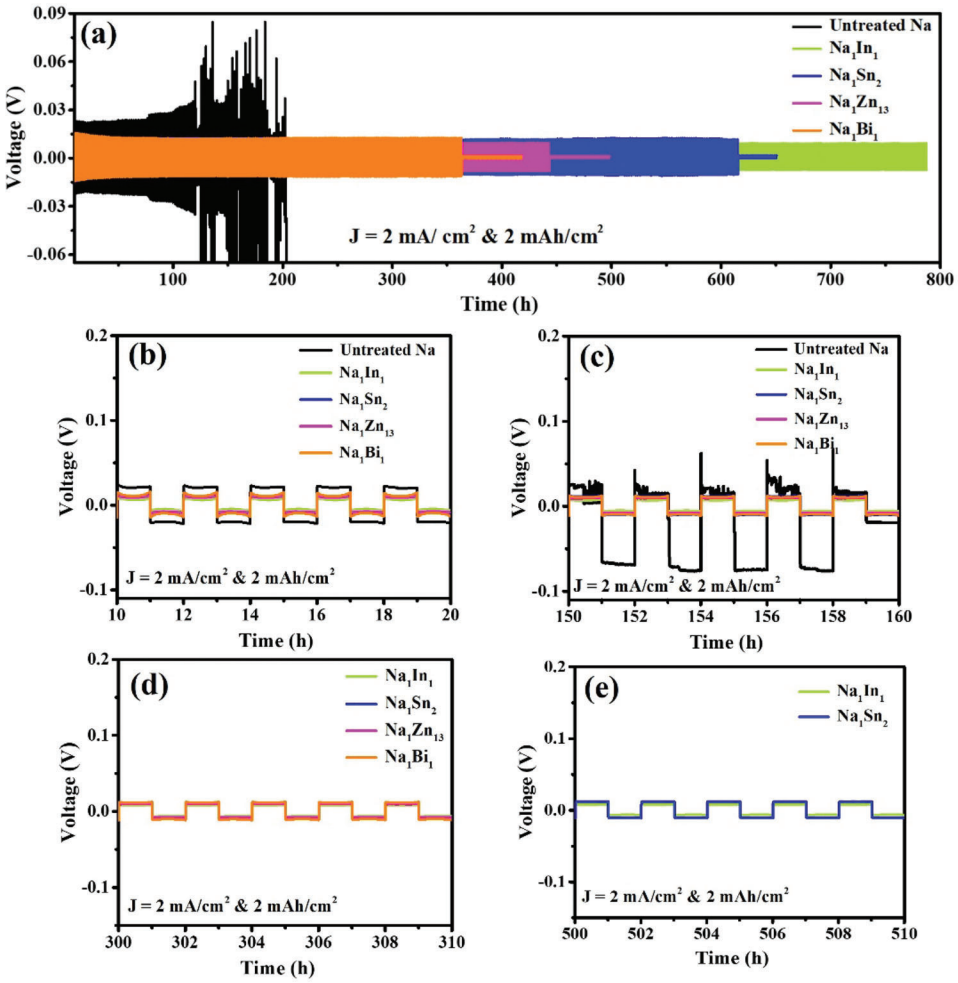

Figure 3. Electrochemical performance of symmetric cells with Na anode and alloy protected Na anode at 2 mA cm^{-2} and capacity of 2 mAh cm^{-2}: a) Voltage vs. time profile comparison, and b–e) Voltage vs. time profiles comparison at difference time range.

Na-Bi is 14 mV, 21 mV, 24 mV, and 27 mV respectively after 300 cycles. Moreover, the surface energy and diffusion barrier required for the Na^+ ion to diffuse across the surface of interlayer also influence the dendrite formation (discussed later in DFT). The Na_1In_1 alloy has the lowest surface energy than Na_1Bi_1, resulting in higher efficiency than other counterparts.[31,43] The thickness of the protective alloy layer on Na metal also influences the electrochemical performance of the metal anode. Therefore, the dependence of the long-term cyclability on the thickness of the Na-In layer is also studied. The thickness of the alloy layer over Na metal can be controlled by treating the Na metal anode with different concentration of the metal chloride solution. Subsequently, the effect of Na-In alloy thickness were studied by treating Na metal anode with low (0.1 M) concentration and high concentration (0.25 M) of indium chloride solution in tetrahydrofuran solvent. The concentration of metal chloride solution greatly influences the thickness and surface flatness of Na-In alloy layer. Na-In metal anode prepared with low and high concentrations (0.1 M and 0.25 M) exhibits high overpotential, uneven plating/stripping, poor cycle life, and instability than Na-In metal anode prepared with 0.15 M indium chloride solution (Figure S5, Supporting Information) The optimized concentration of 0.15 M metal chloride-based electrode demonstrates excellent cyclability, lower overpotential, and dendrite free Na deposition than other concentrations. The low concentration metal chloride solution would result in the formation of unstable and very thin Na-M artificial SEI layer, while high concentration of metal chloride would result in thick Na-M artificial SEI layer over the Na metal, influencing the interphase resistance of metal anode. The Nyquist plots (Figure S6, Supporting Information) of Na-In anode prepared with 0.15 M concentration exhibited lower charge transfer resistance and better interphase properties than Na-In metal anode prepared with other concentrations (0.1 M and 0.25 M). When the Na metal is treated with low concentration of metal chloride solution, the formation of Na-M alloy layer and NaCl layer would be incomplete, leading to unfavorable interface while at high concentration of metal chloride solution, excess of metal chloride salts and NaCl could increase the interface resistance. Also, Table S1 (Supporting Information) compares the performance of the several protective layer over previously studied alloy layer, and observed that the current protective alloy layers are showing the high performance than other protective techniques.

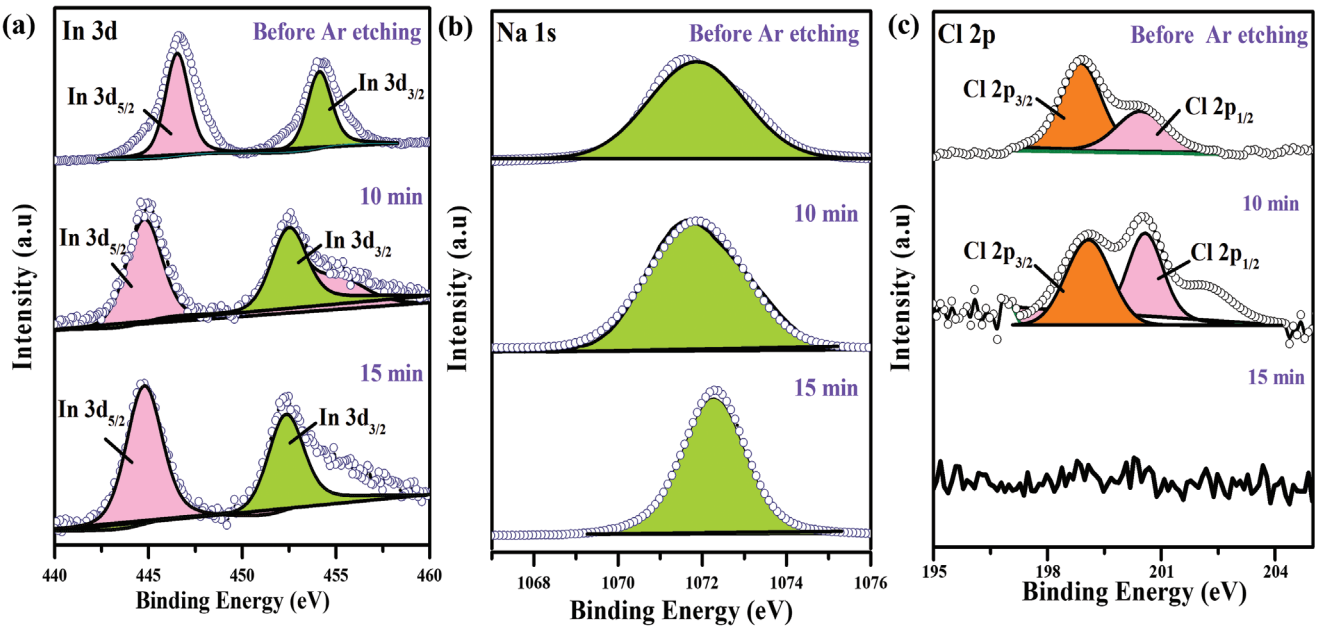

Figure 4. SEI layer formation over Na anode protected with Na_1In_1 alloy after 5th cycle, a) high resolution In3d spectrum b) high resolution Na1s spectrum, and c) high resolution Cl2p spectrum

3.3. SEI Layer Formation

The components of SEI layer, and the change in components of the SEI layer was studied by XPS, to analyze the stability of the Na anode protected with Na-In alloy after cycling (**Figure 4**). We focused on the In3d, Na1s, Cl2p, O1s, and C1s XPS profiles, because Na-In, NaCl and other organic components are one of the key components of the SEI layer. After 5th cycle, the deconvoluted In 3d spectrum at 446.27 eV (In $3d_{5/2}$) and 453.36 eV (In $3d_{3/2}$) in (Figure 4a) shows the predominant contribution from Na_1In_1 alloy layer with a minor contribution from In metal and In_2O_3 before cycling, indicates the presence of mechanical stable alloy type artificial interface layer over Na anode.[44] The Na1s spectrum in (Figure 4b) shows a broad curve at ≈1072 eV due to contributions from NaCl and Na_1In_1 phases. The two peaks at 198.2 and 200.3 eV in the Cl2p spectrum (Figure 4c) were designated to $Cl2p_{3/2}$ and $Cl2p_{1/2}$, respectively, indicating the presence of Na-rich NaCl layer over the Na anode protected with Na-In alloy, helping the facile Na deposition and stripping process.[2,45,46] The C1s and O1s spectrum of Na anode protected Na_1In_1 alloy (Figure S7, Supporting Information) shows the emergence of new organic SEI components for sodium alkoxides after cycling process. The deconvoluted C1s spectra and O1s spectrum after cycling shows the emergence of new functionalities (C–H, C–O, Na–O) over Na anode protected with Na-In alloy. This is mainly attributed to slight reduction of liquid electrolyte over Na-In alloy during initial cycling, helping to form components of natural SEI layer.[11] The origin of the organic components plays a very crucial to provide flexibility to the multifunctional SEI layer at high current and high-capacity conditions. However, the signals of NaCl layer from Cl2p and Na1s spectrum decreased with etching, and completely disappeared after etching process, indicating that the top layer of alloy anode is covered by Na-rich NaCl phase.[47] The Na-ion gets diffused through this Na-rich NaCl and get deposited beneath the alloy layer. The Na-rich NaCl component establishes the necessary potential gradient to drive Na^+ ion diffusion through the alloy layer. Benefiting from the thinner NaCl layer with high elastic modulus, and high electronic resistivity, the hybrid interface can withstand long repeated plating and stripping process. The deconvoluted In3d, Na1s, Cl2p XPS spectrum of Na_1In_1 alloy protected anode after 25th cycle (**Figure 5**) shows the similar pattern as 5th cycle, indicating the presence of robust and stable artificial SEI layer over Na anode that regulates the Na deposition/stripping through facile Na^+ ion diffusion flux.[48,49] The electronically resistive NaCl layer over metal anodes are highly insoluble in organic electrolytes and will hamper electrolyte decomposition on continuous cycling. The formation of ultrathin Na-rich NaCl layer over Na metal anodes plays a dominant role in stabilizing the metal anode. Similar SEI formation trend is noted for other alloy protected anodes as shown in (Figure S8–S10, Supporting Information) and the difference being the type of metal alloy layer over the Na anode.

To understand the origin of the superior performance of Na anode with alloy interface, ex-situ SEM analysis were performed on Pristine Na metal and Na metal with Na_1In_1, Na_1Sn_2, Na_1Zn_{13} Na_1Bi_1 interface after cycling (100 cycles). The SEM images of the pristine Na anode (Figure S11a,b, Supporting Information) revealed a rough surface along with uneven Na deposition, indicating a severe dendrite formation. Such a rough and uneven surface mainly originated from the repeated inhomogeneous Na deposition in host less Na anode with unstable SEI layer. In contrast, the SEM images of Na anode with Na_1In_1, Na_1Sn_2, Na_1Zn_{13}, Na_1Bi_1 interface exhibited a smooth surface without any signs of sodium dendrites as shown in (Figure S11c–f, Supporting Information). The SEM elemental mapping analysis (Figure S12, Supporting Information) of Na-In shows, even after cycling (100 cycles), SEI components (Na, In, Cl) over the Na-In protective layer still remains intact, confirming the mechanical integrity of the

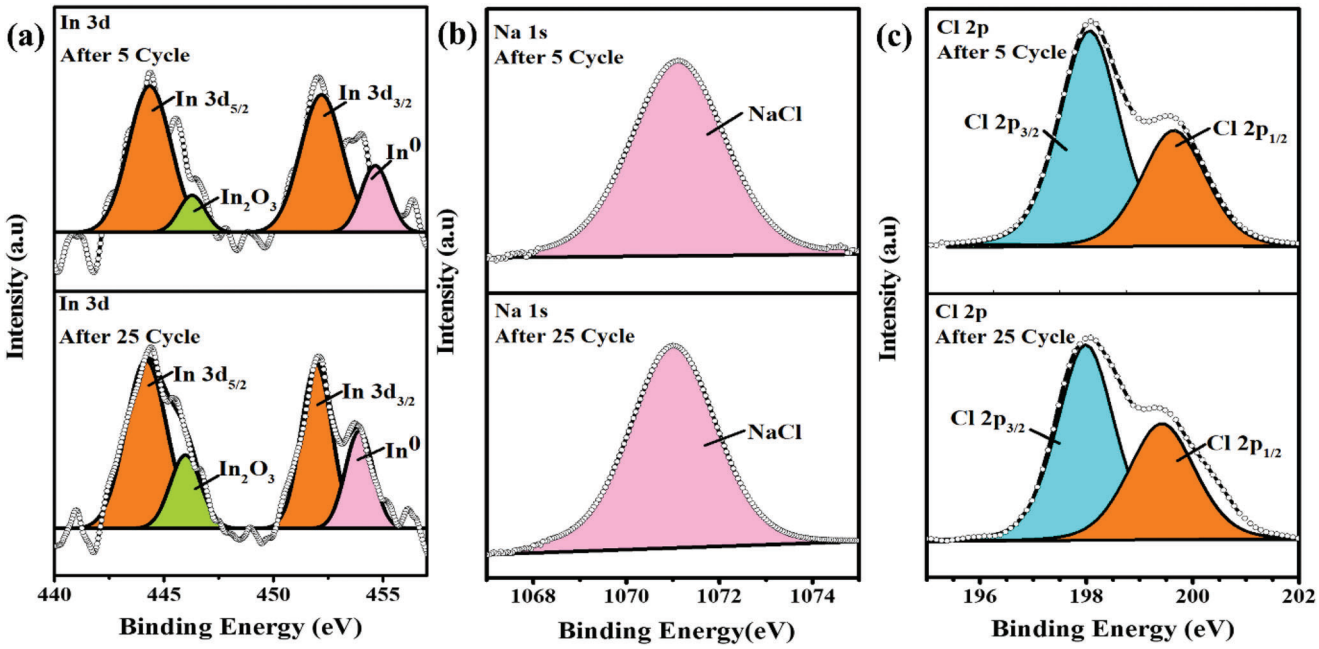

Figure 5. SEI layer formation over Na anode protected with Na_1In_1 alloy after 5th and 25th cycle, a) high resolution In3d spectrum b) high resolution Na1s spectrum, and c) high resolution Cl2p spectrum

alloy anode. This indicates the effective protective of Na anode with hybrid SEI layer comprising Na-rich components and alloy type interface layer.[50]

3.4. Kinetics of Na Metal Deposition/Stripping

To understand the kinetics of the Na deposition/stripping at high current conditions, the stability of pristine Na anode and Na-In protected Na anode were evaluated at current density of 5 mA cm^{-2}. The charge discharge profile in (**Figure 6**a) shows that pristine Na metal has a large overpotential due to resistance in mass transfer at high current conditions, and the overpotential increased with cycles.[39] The bare Na metal anode exhibits unstable behavior after 80 h, much lower than the performance at low current rates. However, Na anode with Na_1In_1 interface exhibited a stable voltage profile with a very low overpotential (19 mV), lower than pristine Na metal. Unlike pristine Na anode, the overpotential of Na anode with Na_1In_1 interface remains same throughout the cycling, and can be cycled efficiently over 266 h. The absence of a voltage drop and voltage fluctuations indicated the presence of a stable interface for Na deposition and low nucleation overpotential to achieve enhanced kinetics.[51]

The cyclic stability of pristine Na anode and Na anode with Na_1In_1 anode is studied in high cell capacity of 5 mAh cm^{-2} and current density of 2 mA cm^{-2}, and the data is presented in (Figure 6b). The pristine sodium anode exhibited uneven plating and stripping after 90 h of cycling with a high overpotential of ≈50 mV. At high capacity testing, sodium metal could settle at a few local spots as dead Na during cycling, which created large grooves and dendrite throughout the stripping process.[52] The Na anode with Na_1In_1 layer performs efficient plating and stripping performances without dendrite formation for over 295 h with low over potential. Since the Na deposition occurred beneath the Na-rich SEI layer, the volume expansion associated with high-capacity Na plating would exert high outward pressure on the SEI layer than low capacity testing. Such stress will lead to breakage of SEI layer at a threshold limit, and lead to fast electrolyte consumption, dendrite formation and early cell failure.[42] Such irregular Na plating/stripping in pristine Na anode generated pressure on the SEI layer followed by the breakage of SEI layer. However, a strong tensile strength from Na_1In_1 layer and flexibility from Na-rich NaCl layer/organic SEI layer helped to withstand the stress and volume expansion exerted during high capacity storage.[53,54] Similarly, Na anode with Na_1Sn_2 interface exhibited even plating and stripping even after 290 h with low overpotential of 21 mV, depicting the role of artificial interface layer for achieving high-capacity Na metal anodes (Figure S13 and S14, Supporting Information). However, Na anode with Na_1Zn_{13} Na_1Bi_1 alloy layers cannot be cycled efficiently over 100 h due to poor mechanical strength of the alloy layers. Nanoindentation studies were carried out using a commercial atomic force microscope to determine the Young's modulus of Na metal and Na-In alloy anode. The binary intermetallic compounds (Na-M) generally have higher mechanical stability than pristine Na metal. The results in Figure S15 (Supporting Information) shows that the Young's modulus of NaIn alloy is ≈8 Gpa, twice higher than pristine Na metal (≈4 Gpa), which is consistent with the claims made in the manuscript. The corresponding average Young's modulus value (32*32 matrix, Hertz model) of Na metal and NaIn alloy is ≈2.2 Gpa, and ≈4.2 Gpa respectively.[54] Therefore, we conclude that the hybrid multifunctional SEI layer comprising mechanically strong alloy component–Na rich NaCl component–organic component improved the cell performance at high current rates and high capacity storage.[35,15]

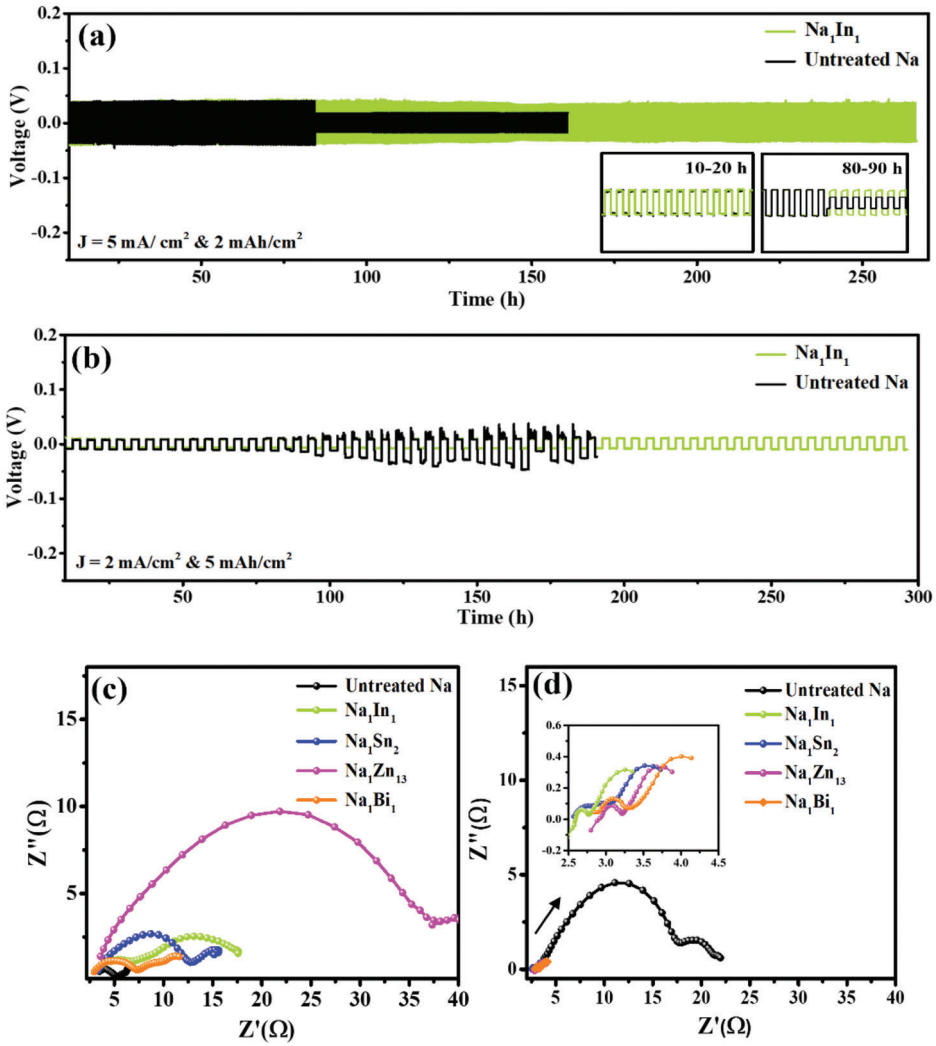

Figure 6. Electrochemical performance of Na anode and Na_1In_1 protected anode at different conditions a) 5 mA cm^{-2} and capacity of 2 mAh cm^{-2}, b) 2 mA cm^{-2} and capacity of 5 mAh cm^{-2}, and Nyquist plots of different anodes c) before cycling, and d) after 75 cycles

To elucidate the effect of the alloy interface layer relative to pristine sodium, we conducted EIS testing. The Nyquist plots of the Na metal anode with interface layer and pristine Na are shown in (Figure 6c,d). The first semicircle in the high-frequency regions of the plots of both pristine Na metal and Na metal alloy interface layer electrodes show the resistance of the SEI layer. The second semicircle in the low-frequency region indicates the charge transfer resistance.[55] The charge transfer resistance of pristine Na anode before cycling was low due to native formed SEI layer after reaction of Na metal with electrolyte. However, after cycling (75 cycles), the interface resistance of pristine Na anode increased significantly (R_{ct} = 17.4 Ω) as Na metal undergoes continuous unwanted side reactions with the electrolyte, resulting in the accumulation of thicker, and poor Na-ion conductive SEI layer. The increasing charge transfer resistance in pristine Na metal anode impedes the kinetics of the Na deposition/stripping process, leading to failure.[30]

The Nyquist plots of Na anode with alloy protective alloy interface shows a higher charge transfer resistance before cycling, due to higher electrical resistivity from originating from metal-alloy interface than pristine Na metal. The interface resistance of Na-M alloys before cycling increases in the following order (Na-Zn< Na-Bi<Na-Sn<Na-In). However, after 75 cycles, the surface of Na anode with protective alloy interface stabilized resulting in reduction of interface resistance. The interface resistance of Na-In, Na-Sn, Na-Zn, and Na-Bi alloys were 2.78 Ω, 2.82 Ω, 3.2 Ω, and 3.4 Ω respectively. This is mainly attributed to stabilization of artificial interface by formation new natural SEI layer after the reaction between Na-M alloy and organic liquid electrolyte. The formation of organic SEI layer components during the initial plating/stripping process increased the interface contact between Na metal–alloy layer–artificial/natural SEI components, thereby reducing any voids or defects in interface layer.[56]The origin of new polar functional groups over the artificial SEI layer after initial cycling can facilitate easy and rapid Na-ion transfer kinetics from electrolyte ions and deposit them below the alloy interface. The small interface resistance in alloy protected Na anode was mainly attributable to the conformal organic and in organic SEI layer that

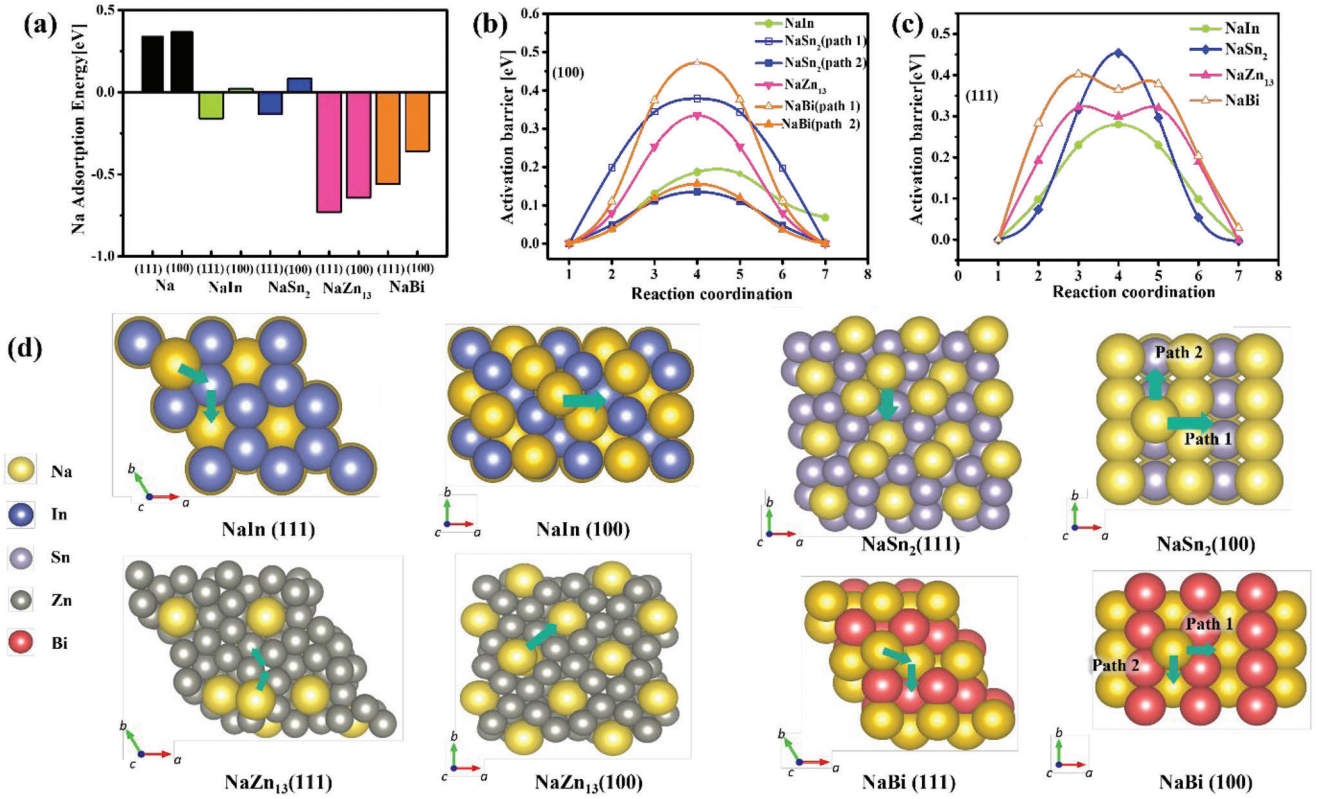

Figure 7. a) Na adsorption energy and diffusion activation barrier for NaIn, $NaSn_2$, $NaZn_{13}$, and NaBi. The activation barrier for (100) plane is shown in the left panel of b), and the activation barrier for (111) plane is shown in the right panel of. c), d) the Na diffusion pathway of each alloy. The green arrows indicate the diffusion pathway.

could enhance the interfacial contact between components of the anode.[57,33] Faster ionic conduction and transportation close to the electrode surface is favorable for achieving low charge transfer resistance, enabling the alloy protected metal anode perform efficiently at high current and high capacity testing conditions. The low and stable interface resistance in Na anode with Na_1In_1 and Na_1Sn_2 enhanced the Na deposition/stripping kinetics and interfacial stability than pristine Na metal and Na_1Zn_{13}/Na_1Bi_1 protected Na metal.[45]

3.5. Density Functional Theory Calculations

We have performed density functional theory (DFT) calculations to understand the origin of the excellent performance of Na anode with alloy protective layer over pristine Na anode.[58]The surface energy and diffusion barrier required for the Na adatom to diffuse across the surface of interlayer were evaluated for Na anode with Na_1In_1, and Na_1Bi_1, $NaSn_2$ and $NaZn_{13}$ alloy interface layers.(**Figure 7**a) shows the evaluated adsorption energies of the Na, NaIn, and NaBi, $NaSn_2$ and $NaZn_{13}$ alloys on the corresponding (100) and (111) planes. Among them, the Na adatoms yielded higher surface energy (0.369 eV and 0.34) than other alloys. The surface energy levels of the other four alloys, namely NaIn (100 and 111), NaBi (100 and 111), $NaSn_2$(100 and 111), $NaZn_{13}$(100 and 111) were (0.021 eV and −0.16 eV), (−0.361 eV and −0.56 eV), (0.082 & −0.133 and) and (−0.645 and −0.731) respectively, making them the favorable candidates with minimum surface energy for Na adsorption. The lower surface energy of the alloys (NaIn, NaBi, $NaSn_2$, and $NaZn_{13}$) relative to that of Na metal clearly indicates that low surface energy is the key factor for facilitating ion diffusion across the surface; and the sodium deposition is inclined toward the alloy surface. The diffusion barrier of Na metal is 0.27 eV, which is excessive for inducing dendrite formation on its surface. As depicted in (Figure 7b,c), the diffusion barriers of NaIn, NaBi, $NaSn_2$ and $NaZn_{13}$ are 0.188 eV, 0.475 eV, 0.13 eV, and 0.335 eV on the (100) plane, and 0.278 eV, 0.368 eV, 0.451 eV, and 0.301 eV on the (111) plane, respectively. As shown in (Figure 7d) atoms arrangement and diffusion pathway for each alloy layers in corresponding planes of (100) & (111). respectively. In which green colored arrows show the different pathways between different adsorption sites. Additionally, the activation energy barrier of pristine Na anode and alloy protected Na anode in different planes (Table S2, Supporting Information) confirms that diffusion kinetics are inclined toward the favorable planes of the alloy, helping to achieve a rapid kinetics in Na anode protected with Na_1In_1 alloy.[30,59,60]

3.6. Full Cell Characterization

Considering the potential practical applications of metal anodes, we assembled a full cell using Na anode with/without Na_1In_1 layer and coupled with $Na_3V_2(PO_4)_3$ (NVP) cathode. The

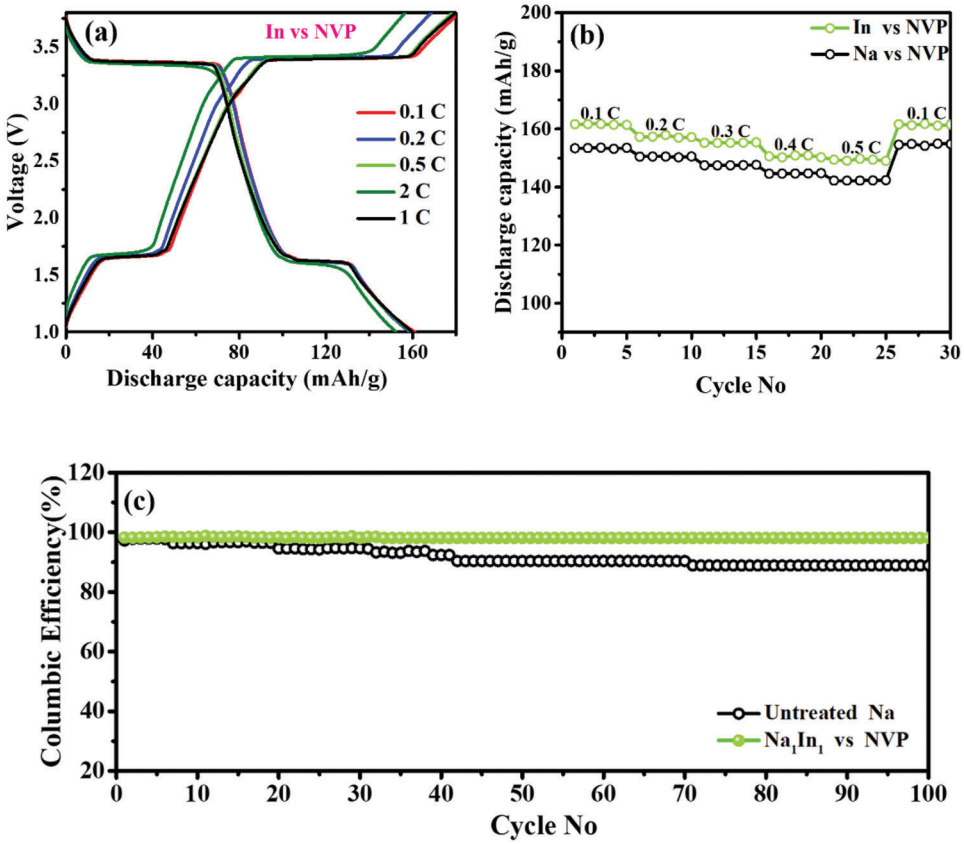

Figure 8. Electrochemical performance of Na-Na_1In_1// $Na_3V_2(PO_4)_3$ full-cell: a) Charge-discharge profiles at different rates, b) rate performance comparison with pristine Na anode, and c) cyclic stability at 1C.

synthesis procedure and properties of NVP cathode used were studied in our previous work.[61] The cells are cycled in the large voltage window (1.0–3.8 V versus Na/Na^+) to extract more Na^+ ions out of NVP cathode and insert more Na^+ ions into the metal anode. The charge discharge profile of the full cell shows two stable plateaus, corresponding to reversible reaction between $NaV_2(PO_4)_3$ and $Na_4V_2(PO_4)_3$ phases (**Figure 8**a). The discharge capacity of full-cell at 0.1, 0.5, 1.0, and 2.0 C was 161, 157, 155, 151, and 150 mAh g^{-1}(Figure 8b) respectively. The capacity obtained with Na_1In_1 anode is much higher than pristine Na at all C rates, and also, they exhibited a low overpotential than pristine Na metal anode. Moreover, the full-cell will Na_1In_1 layer displayed a stable charge-discharge behavior upon cycling. These results further confirm that the hybrid multifunctional interfaces aided the formation of a stable SEI layer over Na metal anode, thereby inhibiting the unwanted consumption of the electrolyte. In contrast, the cell with pristine Na metal anode shows poor cyclic stability and highly fluctuating columbic efficiency due to unwanted electrolyte reaction from highly reactive Na metal (Figure 8c).

4. Conclusion

In summary, we have demonstrated that a Series of hybrid multifunctional interfaces (Na_1In_1, Na_1Sn_2, and Na_1Zn_{13} Na_1Bi_1) made by a simple self-alloying reaction as artificial SEI layer for providing stable interface in Na metal anode. The surface energy of the protective alloys relative to bare Na metal is the key factor for facilitating facile ion diffusion across the interface. The hybrid Na-ion conducting organic-inorganic SEI components can facilitate uniform Na deposition by regulating the Na-ion flux with a low overpotential than pristine Na metal. The mechanically strong Na-In alloy with Na rich NaCl phase can efficiently drive large deposition (10 mAh) of Na metal under the protective alloys. Moreover, the hybrid SEI provides a highly flexible and dense membrane to accommodates the volume changes, regulate the Na^+ ion flux, and reduces the local current density to achieve efficient Na deposition at high current (5 mA cm^{-2}) and withstand repeated Na deposition and stripping process for ≈800 h. The lower surface energy of Na_1In_1 alloys relative to that of Na metal and Na_1Bi_1 alloy facilitates facile ion diffusion across the surface; and the deposition is inclined toward the alloy surface. Our finding is significant that it provides facile surface stabilization strategy for dendrite free Na metal anode, and opens up a promising research direction for development of high energy density sodium metal batteries.

Supporting Information

Supporting Information is available from the Wiley Online Library or from the author.

Acknowledgements

This work was supported by the National Research Foundation of Korea (NRF) grant funded by the Korean government (Ministry of Science, ICT & Future Planning) (No. RS-2023-00208361). Dr. Ranjith Thangavel acknowledges the support from Science and Engineering Research Board (SERB), a statutory body of the Department of Science & Technology (DST), Govt. of India, through the Start-up Research Grant (SRG/2022/000642). S.H. acknowledges the financial support for AFM experiments from the KAIST-funded Global Singularity Research Program for 2023.

Conflict of Interest

The authors declare no conflict of interest.

Data Availability Statement

The data that support the findings of this study are available from the corresponding author upon reasonable request.

Keywords

artificial SEI layer, dendrites, density functional theory, sodium metal anode, solid electrolyte interphase

Received: January 5, 2023
Revised: May 16, 2023
Published online: June 17, 2023

[1] B. Lee, E. Paek, D. Mitlin, S. W. Lee, *Chem. Rev.* **2019**, *119*, 5416.
[2] X. Zheng, H. Fu, C. Hu, H. Xu, Y. Huang, J. Wen, H. Sun, W. Luo, Y. Huang, *J. Phys. Chem. Lett.* **2019**, *10*, 707.
[3] Q. Chen, H. He, Z. Hou, W. Zhuang, T. Zhang, Z. Sun, L. Huang, *J. Mater. Chem. A* **2020**, *8*, 16232.
[4] B. Sun, P. Xiong, U. Maitra, D. Langsdorf, K. Yan, C. Wang, J. Janek, D. Schröder, G. Wang, *Adv. Mater.* **2019**,*30*,1903891.
[5] W. Luo, L. Hu, *ACS Cent. Sci.* **2015**, *1*, 420.
[6] A. Wang, X. Hu, H. Tang, C. Zhang, S. Liu, Y. W. Yang, Q. H. Yang, J. Luo, *Angew. Chemie – Int. Ed.* **2017**, *56*, 11921.
[7] Y. Zhao, K. R. Adair, X. Sun, *Energy Environ. Sci.* **2018**, *11*, 2673.
[8] J. Lee, J. Kim, S. Kim, C. Jo, J. Lee, *Mater. Adv.* **2020**, *1*, 3143.
[9] G. Yan, S. Mariyappan, G. Rousse, Q. Jacquet, M. Deschamps, R. David, B. Mirvaux, J. W. Freeland, J. M. Tarascon, *Nat. Commun.* **2019**, *10*, 585.
[10] D. I. Iermakova, R. Dugas, M. R. Palacín, A. Ponrouch, *J. Electrochem. Soc.* **2015**, *162*, A7060.
[11] Z. W. Seh, J. Sun, Y. Sun, Y. Cui, *ACS Cent. Sci.* **2015**, *1*, 449.
[12] E. Matios, H. Wang, C. Wang, W. Li, *Ind. Eng. Chem. Res.* **2019**, *58*, 9758.
[13] T. S. Wang, Y. Liu, Y. X. Lu, Y. S. Hu, L. Z. Fan, *Energy Storage Mater.* **2018**, *15*, 274.
[14] S. Liu, S. Tang, X. Zhang, A. Wang, Q. H. Yang, J. Luo, *Nano Lett.* **2017**, *17*, 5862.
[15] Q. Lu, A. Omar, L. Ding, S. Oswald, M. Hantusch, L. Giebeler, K. Nielsch, D. Mikhailova, *J. Mater. Chem. A* **2021**, *9*, 9038.
[16] M. Mandl, J. Becherer, D. Kramer, R. Mönig, T. Diemant, R. J. Behm, M. Hahn, O. Böse, M. A. Danzer, *Electrochim. Acta* **2020**, *354*, 2019.
[17] G. Li, X. Lou, C. Peng, C. Liu, W. Chen, *Chem. Synth.* **2022**, *2*, 16.
[18] E. Peled, S. Menkin, *J. Electrochem. Soc.* **2017**, *164*, A1703.
[19] H. Tan, D. Chen, X. Rui, Y. Yu, *Adv. Funct. Mater.* **2019**, *29*, 1808745.
[20] S. Wang, Y. Jie, Z. Sun, W. Cai, Y. Chen, F. Huang, Y. Liu, X. Li, R. Du, R. Cao, G. Zhang, S. Jiao, *ACS Appl. Energy Mater.* **2020**, *3*, 8688.
[21] Y. Fang, X. Y. Yu, X. W. (David) Lou, *Matter* **2019**, *1*, 90.
[22] W. Liu, P. Liu, D. Mitlin, *Adv. Energy Mater.* **2020**, *10*, 2002297.
[23] V. Kumar, A. Y. S. Eng, Y. Wang, D. T. Nguyen, M. F. Ng, Z. W. Seh, *Energy Storage Mater.* **2020**, *29*, 1.
[24] Q. Lu, A. Omar, M. Hantusch, S. Oswald, L. Ding, K. Nielsch, D. Mikhailova, *Appl. Surf. Sci.* **2022**, *600*, 154168.
[25] X. Liang, Q. Pang, I. R. Kochetkov, M. S. Sempere, H. Huang, X. Sun, L. F. Nazar, *Nat. Energy* **2017**, *2*, 17119.
[26] G. Kresse, J. Furthmüller, *Phys. Rev. B – Condens. Matter Mater. Phys.* **1996**, *54*, 11169.
[27] H. J. M. James, D. Pack, *J. Chem. Inf. Model.* **1977**, *16*, 1748.
[28] L. Zhang, Y. Xia, H. Yang, S. Xiao, J. Zhou, Y. Cao, T. Qian, *APL Mater.* **2022**, *10*, 070901.
[29] H. Wang, Y. Wu, Y. Wang, T. Xu, D. Kong, Y. Jiang, D. Wu, Y. Tang, X. Li, C. S. Lee, *Nano-Micro Lett.* **2022**, *14*, 50.
[30] R. Wang, J. Yu, J. Tang, R. Meng, L. F. Nazar, L. Huang, X. Liang, *Energy Storage Mater.* **2020**, *32*, 178.
[31] S. Li, Y. Huang, W. Ren, X. Li, M. Wang, H. Cao, *Chem. Eng. J.* **2021**, *422*, 129911.
[32] B. Sun, P. Li, J. Zhang, D. Wang, P. Munroe, C. Wang, P. H. L. Notten, G. Wang, *Adv. Mater.* **2018**, *30*, 1801344.
[33] W. Luo, C. F. Lin, O. Zhao, M. Noked, Y. Zhang, G. W. Rubloff, L. Hu, *Adv. Energy Mater.* **2017**, *7*, 1601526.
[34] X. Lai, Z. Xu, X. Yang, Q. Ke, Q. Xu, Z. Wang, Y. Lu, Y. Qiu, *Adv. Energy Mater.* **2022**, *12*, 2103540.
[35] M. J. Wang, J. Y. Chang, J. B. Wolfenstine, J. Sakamoto, *Materialia* **2020**, *12*, 100792.
[36] Z. Xu, J. Yang, T. Zhang, L. Sun, Y. Nuli, J. Wang, S. ichi Hirano, *Adv. Funct. Mater.* **2019**, *29*, 1901924.
[37] Y. Liu, D. Lin, P. Y. Yuen, K. Liu, J. Xie, R. H. Dauskardt, Y. Cui, *Adv. Mater.* **2017**, *29*, 1605531.
[38] Y. Zhao, X. Yang, L. Y. Kuo, P. Kaghazchi, Q. Sun, J. Liang, B. Wang, A. Lushington, R. Li, H. Zhang, X. Sun, *Small* **2018**, *14*, 1703717.
[39] X. Zhang, A. Wang, X. Liu, J. Luo, *Acc. Chem. Res.* **2019**, *52*, 3223.
[40] Y. Li, W. Huang, Y. Li, A. Pei, D. T. Boyle, Y. Cui, *Joule* **2018**, *2*, 2167.
[41] K. Thanner, A. Varzi, D. Buchholz, S. J. Sedlmaier, S. Passerini, *ACS Appl. Mater. Interfaces* **2020**, *12*, 32851.
[42] C. Zou, X. Zhang, Y. Huang, L. Zhao, W. Ren, Z. Zhao, J. Liu, X. Li, M. Wang, B. Guo, Y. Lin, *Electrochim. Acta* **2022**, *433*, 141245.
[43] G. Hou, C. Ci, H. Guo, X. Zhang, Q. Sun, J. Cheng, D. Salpekar, Q. Ai, L. Chen, A. B. Puthirath, K. Kato, S. C. Pardo, R. Vajtai, G. Babu, L. Ci, P. M. Ajayan, *Chem. Eng. J.* **2020**, *391*, 123542.
[44] P. Deminskyi, P. Rouf, I. G. Ivanov, H. Pedersen, *J. Vac. Sci. Technol. A* **2019**, *37*, 020926.
[45] J. Song, G. Jeong, A. J. Lee, J. H. Park, H. Kim, Y. J. Kim, *ACS Appl. Mater. Interfaces* **2015**, *7*, 27206.
[46] T. Li, U. Gulzar, X. Bai, M. Lenocini, M. Prato, K. E. Aifantis, C. Capiglia, R. P. Zaccaria, *ACS Appl. Energy Mater.* **2019**, *2*, 860.
[47] C. Yan, X. B. Cheng, Y. Tian, X. Chen, X. Q. Zhang, W. J. Li, J. Q. Huang, Q. Zhang, *Adv. Mater.* **2018**, *30*, 1870181.
[48] H. Liu, X.-B. Cheng, J.-Q. Huang, S. Kaskel, S. Chou, H. S. Park, Q. Zhang, *ACS Mater. Lett.* **2019**, *1*, 217.
[49] L. Gao, J. Chen, Q. Chen, X. Kong, *Sci. Adv.* **2022**, *8*, eabm4606.
[50] Z. Hou, W. Wang, Q. Chen, Y. Yu, X. Zhao, M. Tang, Y. Zheng, Z. Quan, *ACS Appl. Mater. Interfaces* **2019**, *11*, 37693.
[51] K. J. Harry, D. T. Hallinan, D. Y. Parkinson, A. A. MacDowell, N. P. Balsara, *Nat. Mater.* **2014**, *13*, 69.
[52] S. Jiao, J. Zheng, Q. Li, X. Li, M. H. Engelhard, R. Cao, J. G. Zhang, W. Xu, *Joule* **2018**, *2*, 110.
[53] E. A. Il'ina, K. V. Druzhinin, E. D. Lyalin, M. S. Plekhanov, I. I. Talankin, B. D. Antonov, A. A. Pankratov, *J. Mater. Sci.* **2022**, *57*, 1291.

[54] K. Kuriyama, S. Saito, K. Iwamura, *J. Phys. Chem. Solids* **1979**, *40*, 457.
[55] B. Moorthy, J. H. Kim, H. W. Lee, D. K. Kim, *Energy Storage Mater.* **2020**, *24*, 602.
[56] Y. Wang, H. Dong, N. Katyal, H. Hao, P. Liu, H. Celio, G. Henkelman, J. Watt, D. Mitlin, *Adv. Mater.* **2022**, *34*, 2106572.
[57] L. Fan, X. Li, *Nano Energy* **2018**, *53*, 630.
[58] W. Zhao, M. Guo, Z. Zuo, X. Zhao, H. Dou, Y. Zhang, S. Li, Z. Wu, Y. Shi, Z. Ma, X. Yang, *Engineering* **2022**, *42*, 87.
[59] Z. Li, H. Bin Wu, X. W. Lou, *Energy Environ. Sci.* **2016**, *9*, 3061.
[60] H. Yuan, J. Nai, H. Tian, Z. Ju, W. Zhang, Y. Liu, X. Tao, X. W. Lou, *Sci. Adv.* **2020**, *6*, eaaz3112.
[61] R. Thangavel, K. Kaliyappan, K. Kang, X. Sun, Y.-S. Lee, **2016**, *6*, 1502199.